Kinesin-12 motors cooperate to suppress microtubule catastrophes and drive the formation of parallel microtubule bundles

Hauke Drechsler[a,1] and Andrew D. McAinsh[a,1]

[a]Centre for Mechanochemical Cell Biology, Division of Biomedical Cell Biology, Warwick Medical School, University of Warwick, Coventry CV4 7AL, United Kingdom

Edited by Ronald D. Vale, Howard Hughes Medical Institute and University of California, San Francisco, CA, and approved February 9, 2016 (received for review August 19, 2015)

Human Kinesin-12 (hKif15) plays a crucial role in assembly and maintenance of the mitotic spindle. These functions of hKif15 are partially redundant with Kinesin-5 (Eg5), which can cross-link and drive the extensile sliding of antiparallel microtubules. Although both motors are known to be tetramers, the functional properties of hKif15 are less well understood. Here we reveal how single or multiple Kif15 motors can cross-link, transport, and focus the plus-ends of intersecting microtubules. During transport, Kif15 motors step simultaneously along both microtubules with relative microtubule transport driven by a velocity differential between motor domain pairs. Remarkably, this differential is affected by the underlying intersection geometry: the differential is low on parallel and extreme on antiparallel microtubules where one motor domain pair becomes immobile. As a result, when intersecting microtubules are antiparallel, canonical transport of one microtubule along the other is allowed because one motor is firmly attached to one microtubule while it is stepping on the other. When intersecting microtubules are parallel, however, Kif15 motors can drive (biased) parallel sliding because the motor simultaneously steps on both microtubules that it cross-links. These microtubule rearrangements will focus microtubule plus-ends and finally lead to the formation of parallel bundles. At the same time, Kif15 motors cooperate to suppress catastrophe events at polymerizing microtubule plus-ends, raising the possibility that Kif15 motors may synchronize the dynamics of bundles that they have assembled. Thus, Kif15 is adapted to operate on parallel microtubule substrates, a property that clearly distinguishes it from the other tetrameric spindle motor, Eg5.

Kinesin-12 | Kif15 | mitosis | mitotic spindle

Accurate chromosome segregation during mitosis requires the assembly of a microtubule-based spindle with bipolar geometry. Following assembly, the spindle must be maintained in a bipolar state before being remodeled throughout anaphase and cytokinesis. These events are contingent on the dynamic nature of microtubules and multiple force-generating molecular motors (1). The initial step in spindle assembly involves the separation of the duplicated centrosomes during prophase (2). In human cells, this event is absolutely dependent on Kinesin-5 Eg5 (3, 4). It is thought that Eg5 cross-links and slides apart astral microtubules that project from one centrosome toward the other, thereby pushing the centrosomes apart. This model is based on key in vitro experiments showing that the Eg5 motor is a bipolar tetramer (5), which can cross-link and drive the extensile sliding of antiparallel microtubules in vitro (6, 7).

Eg5 also contributes to the force equilibrium in prometaphase/metaphase that maintains the bipolar spindle geometry (8). As in centrosome separation, Eg5 generates an outward pushing force by sliding apart antiparallel overlapping nonkinetochore microtubules. However, Eg5 is not essential for spindle maintenance because a second motor, Kinesin-12 Kif15, can compensate for loss of Eg5 activity (9, 10). Kif15 is not required for centrosome separation in prophase, although overexpression of the motor can also drive spindle formation during prometaphase—even in the absence of Eg5 activity (9, 11). The redundancy of Eg5 and Kif15 led to the idea that Kif15 functions in close analogy to Eg5 and slides apart antiparallel overlaps of interpolar microtubules, thereby generating outward-pushing forces on the centrosomes (9). However, this model is not compatible with recent cell biological experiments: First, Kif15 mainly localizes to and acts on kinetochore fibers (k-fibers: bundles of parallel microtubules that connect spindle poles and kinetochores) rather than on nonkinetochore microtubules that can form antiparallel overlaps (11). Second, Kif15 motors generate forces that counteract Eg5-dependent forces (11). Nevertheless, such cell biological approaches are limited in that they cannot alone reveal the underlying mechanism(s) by which the Kif15 motor operates in vivo. Hence, a detailed biochemical and biophysical understanding of this motor is essential.

As a first step, we recently provided an initial biochemical characterization of full-length human Kif15 motors in vitro (12). We found that at physiological ionic strength hKif15 motors exist as tetramers. These motors are highly processive, capable of switching tracks at microtubule intersections, and can step against loads of up to 3.5 pN (12). Kif15 tetramers can also mediate the cross-linking of two microtubules, but give rise to very little microtubule sliding, except for episodes of short duration transport of short microtubules (12). A second study recently reported that a dimeric Kif15 missing the carboxyl-terminal half of the protein is also able to drive microtubule transport (13). One limitation of both studies is that they use stabilized microtubules rather than dynamic microtubules. As dynamicity is a main hallmark of the

Significance

During cell division, molecular motors from the kinesin superfamily, in particular Kinesin-12 (Kif15) and Kinesin-5 (Eg5), play a crucial role in formation of the spindle—a bipolar microtubule array that is essential for accurate chromosome segregation. While Eg5 is well studied, the mechanism by which Kif15 maintains spindle bipolarity in the absence of Eg5 is unknown. In this work we reconstitute Kif15 motors on dynamic microtubules in vitro. We reveal that Kif15 is a multi-function motor that cross-links microtubules and drives transport of one along the other, which results in the formation of parallel microtubule bundles. Additionally, motors track the microtubule tips, maintaining them in a growing state, which can synchronize microtubule dynamics within a bundle.

Author contributions: H.D. and A.D.M. designed research; H.D. performed research; H.D. analyzed data; and H.D. and A.D.M. wrote the paper.

The authors declare no conflict of interest.

This article is a PNAS Direct Submission.

Freely available online through the PNAS open access option.

[1]To whom correspondence may be addressed. Email: a.d.mcainsh@warwick.ac.uk or h.drechsler@warwick.ac.uk.

This article contains supporting information online at www.pnas.org/lookup/suppl/doi:10.1073/pnas.1516370113/-/DCSupplemental.

mitotic spindle, important features of hKif15 activity might be missed by in vitro approaches using stabilized microtubules. For example, the long plus-end dwell time of hKif15 motors suggests that the motor may interfere with microtubule dynamics (12). We therefore aimed to study the behavior of hKif15 motors in networks of dynamic microtubules in vitro.

Results

hKif15 Motors Track Polymerizing, but Not Depolymerizing, Microtubule Ends. We previously reported that single hKif15-eGFP homotetramers moving on stabilized microtubules dwell for extended periods of time at the microtubule plus-end (12). This observation prompted us to investigate whether such behavior also occurs on dynamic microtubules and whether it influences their plus-end dynamics. As the buffer conditions (i.e., BRB60: 60 mM Pipes, 1 mM $MgCl_2$, 1 mM EGTA, pH = 6.8) and temperature (35 °C) required for microtubules to undergo dynamic instability differ from our previous work (12), we confirmed that Kif15 exists as a monodispersed, tetrameric species under these new conditions (Figs. S1 and S2). However, a recent characterization of a dimeric hKif15 version (13) raised the question (see also ref. 14) as to which oligomerization state of hKif15 is physiologically relevant. We therefore compared our recombinant hKif15 with endogenous hKif15 from human cell extracts. Both proteins migrate as a monodispersed population with a sedimentation coefficient of ~12 S in a 5–40% glycerol gradient at a physiological ionic strength (Fig. S1 *C* and *D*). These data show that hKif15 is a fully functional tetramer at physiological ionic strength in vitro as well as in cell extracts, thus providing strong evidence that this is the physiologically relevant form of the motor.

In an initial in vitro experiment we grew microtubules with X-rhodamine–labeled tubulin from surface-bound HiLyte 647-labeled seeds in the presence of 5 nM hKif15-eGFP (tetramer) and followed microtubule growth and motor movement for 5 min by Total Internal Reflection Fluorescence (TIRF) microscopy. Kymographs derived from line scans along the microtubule axis reveal that the motors are indeed able to track the growing microtubule plus-ends (Fig. 1*A*, *Upper*). Motors were observed to accumulate at the plus-ends because their speed (502 ± 8.9 nm·s^{-1}, median ± SEM, Fig. S2*B*) exceeds that of the growing tip (22 ± 1.3 nm·s^{-1}, median ± SEM, Fig. 2*B*). As expected, hKif15 motors failed to track the polymerizing end when motor motility was inhibited by the nonhydrolyzable ATP analog AMP-PNP (Fig. 1*A*, *Lower*).

Although hKif15 motors reliably tracked the polymerizing plus-end, they were never observed on the tips of depolymerizing microtubules. Without exception, plus-end–tracking hKif15-eGFP particles immediately leave the microtubule lattice once a catastrophe event occurs (Figs. 1*A* and 2*A*; Fig. S3*A*). Furthermore, hKif15 motors that step onto a depolymerizing plus-end are also stripped off the lattice immediately (Fig. 1*A*, magnification in *Upper Right*, white arrowheads). This stringency is surprising, given that the motor is able to walk for a short distance toward the minus-end and able to roam the plus-end proximal lattice by diffusion (ref. 12 and Fig. S2*A*, kymograph no. 3). Thus, hKif15 motors would be expected to occasionally track the plus-end during microtubule depolymerization.

One possible explanation for this behavior is that structural changes in the tip following catastrophe, such as the bending of protofilaments (15), affect the hKif15–microtubule interaction. To test this idea directly, we compared the affinity of hKif15 motors for taxol-stabilized microtubules and short curved protofilaments, which have been assembled in the presence of vinblastine (16) (see Fig. 1*B*, *Lower panels*, for geometry of the respective tubulin assemblies). Strikingly, hKif15 shows no significant binding to vinblastine curls irrespective of the microtubule concentration (Fig. 1*B* and Fig. S1*E*). To test whether impaired binding to vinblastine curls is a general behavior of kinesins, we included tetrameric full-length hEg5 as an internal control. From

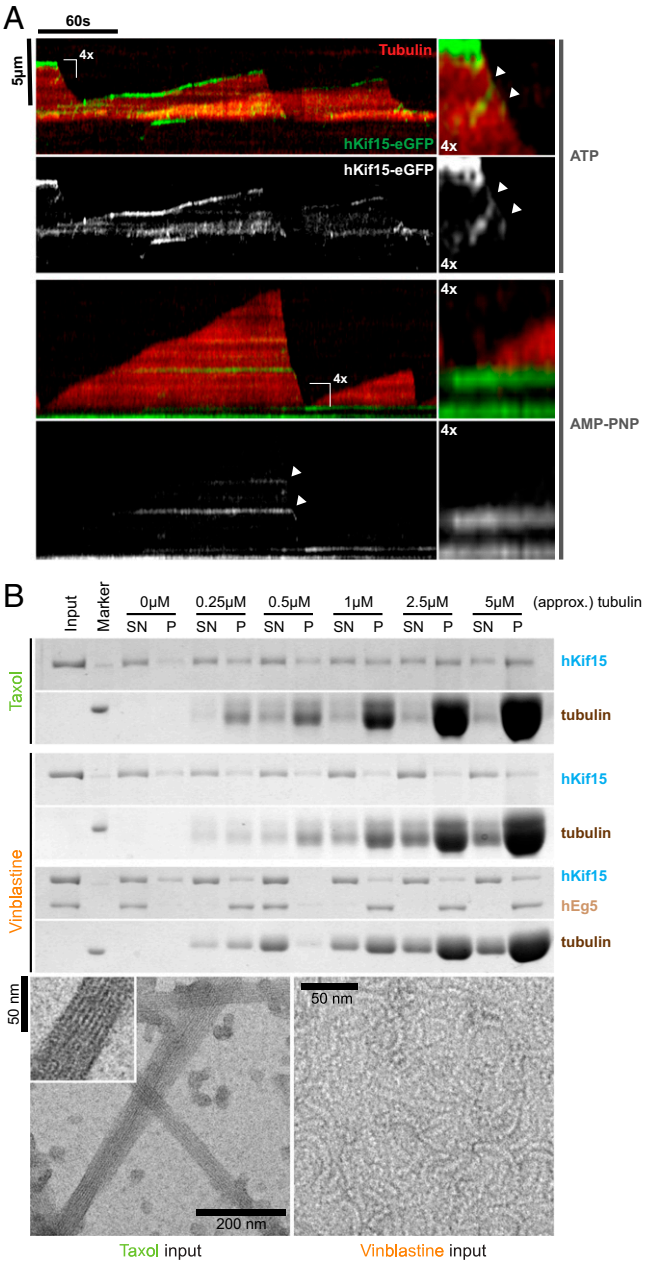

Fig. 1. hKif15 motors actively track polymerizing, but not depolymerizing, microtubule ends. (*A*) Kymographs showing the behavior of hKif15-eGFP motors (at 5 nM) on dynamic microtubules in the presence of 1.7 mM ATP (*Top*) or nonhydrolyzable AMP-PNP (*Bottom*). Plus-ends of microtubules are oriented toward the top. (*Top Right*) Fourfold magnification showing motors walking into a depolymerizing microtubule plus-end (white arrowheads). (*Bottom Right*) Fourfold magnification showing the microtubule growing out from a hKif15-eGFP-rich area. (*B*, *Top*) Coomassie-stained SDS/PAGE gels showing cosedimentation experiments of recombinant hKif15 (and hEg5, both at 15 nM) in the presence of straight microtubules (Taxol) or curved tubulin filaments (Vinblastine) at the indicated tubulin concentration. SN, supernatant, P, pellet. (*Bottom*) Negative-stain electron micrographs showing the geometry of tubulin polymers used for the experiment. (*Inset*) Magnification of the microtubule fine structure.

an equimolar hKif15/hEg5 mix, hEg5 is cosedimented efficiently by vinblastine-induced microtubule curls, whereas hKif15 again remains in the supernatant at any tubulin concentration tested (Fig. 1*B*). Thus, the observed effect seems to be specific to hKif15. We conclude that the curvature of depolymerizing microtubules is

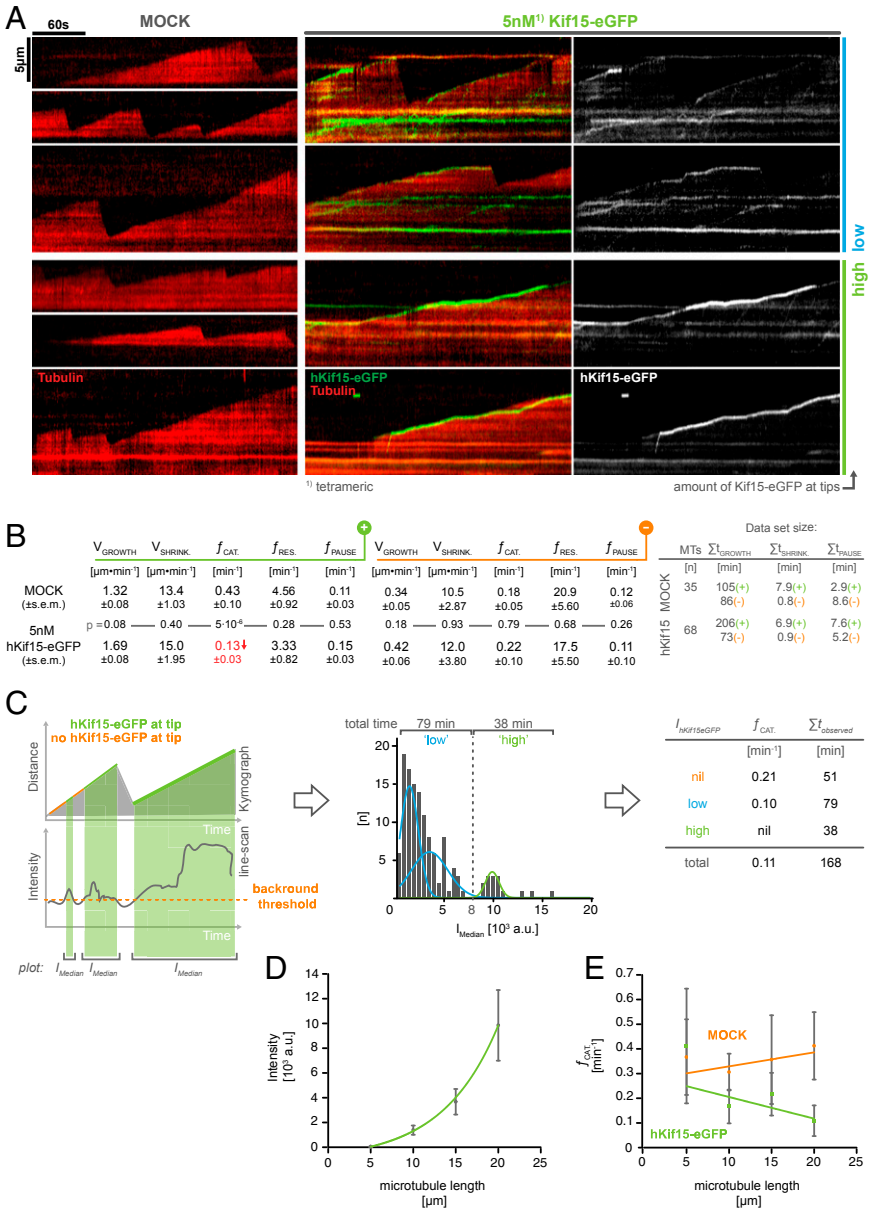

	V_{GROWTH} [µm•min⁻¹]	$V_{SHRINK.}$ [µm•min⁻¹]	$f_{CAT.}$ [min⁻¹]	$f_{RES.}$ [min⁻¹]	f_{PAUSE} [min⁻¹]	V_{GROWTH} [µm•min⁻¹]	$V_{SHRINK.}$ [µm•min⁻¹]	$f_{CAT.}$ [min⁻¹]	$f_{RES.}$ [min⁻¹]	f_{PAUSE} [min⁻¹]
MOCK (±s.e.m.)	1.32 ±0.08	13.4 ±1.03	0.43 ±0.10	4.56 ±0.92	0.11 ±0.03	0.34 ±0.05	10.5 ±2.87	0.18 ±0.05	20.9 ±5.60	0.12 ±0.06
p =	0.08	0.40	$5 \cdot 10^{-6}$	0.28	0.53	0.18	0.93	0.79	0.68	0.26
5nM hKif15-eGFP (±s.e.m.)	1.69 ±0.08	15.0 ±1.95	0.13↓ ±0.03	3.33 ±0.82	0.15 ±0.03	0.42 ±0.06	12.0 ±3.80	0.22 ±0.10	17.5 ±5.50	0.11 ±0.10

	MTs [n]	Σt_{GROWTH} [min]	$\Sigma t_{SHRINK.}$ [min]	Σt_{PAUSE} [min]
MOCK	35	105(+) 86(-)	7.9(+) 0.8(-)	2.9(+) 8.6(-)
hKif15	68	206(+) 73(-)	6.9(+) 0.9(-)	7.6(+) 5.2(-)

$I_{hKif15eGFP}$	$f_{CAT.}$ [min⁻¹]	$\Sigma t_{observed}$ [min]
nil	0.21	51
low	0.10	79
high	nil	38
total	0.11	168

Fig. 2. hKif15 motors cooperate to suppress catastrophe at microtubule plus-ends. (*A*) Kymographs showing the dynamicity of microtubule plus-ends in the absence (*Left*, MOCK) or presence of 5 nM Kif15-eGFP (*Right*) and 1.7 mM ATP. Two examples of each "low" and "high" amounts of plus-end–tracking motors are shown. (*B*) A global analysis of microtubule dynamicity parameters in the absence and presence of 5 nM hKif15-eGFP, subdivided into results for the plus-end (green) and the minus end (orange). V, velocity; *f*, frequency; *t*, time. The SE of the mean for each value is given and was calculated from the mean of the respective values per microtubule. Values are averages from multiple chambers. (*C*, *Left*) Scheme visualizing the procedure to subsample data for a correlation between the intensity of plus-end–tracking hKif15-eGFP particles and the catastrophe frequency at the microtubule plus-ends. See *hKif15 Motors Cooperate to Inhibit Microtubule Catastrophe* for a more detailed description. (*Middle*) Frequency distribution of median intensities (over time) of plus-end–tracking hKif15-eGFP motors (coherent phases >5 seconds). Due to the split intensity distribution, data showing end-tracking motors were subdivided into phases with "low" (<8,000 arbitrary units) and "high" (>8,000 arbitrary units) end-tracking motor amounts. (*Right*) The catastrophe frequency for the categories defined in the *Middle* panel. (*D*) Graph depicting the average hKif15-eGFP intensity tracking the plus-end during a microtubule growth phase in dependency on the average microtubule length during that growth event. Data are binned in 5-µm steps. Error bars indicate the SE of mean. (*E*) Graph showing the correlation of catastrophe events and the average microtubule length during a growth phase. The green linear fit represents measurements in the presence of 5 nM hKif15-eGFP, and the orange linear fit describes the behavior in a MOCK setup. Data are binned in 5-µm steps. Error bars indicate the SE of mean.

likely to be the reason for hKif15 dissociation from microtubule plus-ends following a catastrophe event. As a result, hKif15 specifically tracks the growing plus-ends of microtubules.

hKif15 Motors Cooperate to Inhibit Microtubule Catastrophe. To investigate whether tip-tracking hKif15 influences plus-end dynamics, we determined the speed of microtubule growth/shrinkage and the frequency of catastrophe/rescue events in the presence or absence of the motor (Fig. 2 *A* and *B*). In this analysis we also included the microtubule minus-ends, on which hKif15 is absent and thereby serve as an internal control for basal microtubule dynamicity. This analysis showed that 5 nM hKif15-eGFP selectively reduces the catastrophe frequency from 0.43 ± 0.10 min^{-1} in control to 0.13 ± 0.03 min^{-1} (45 catastrophes in

105 min vs. 26 catastrophes in 206 min, $P = 5{\cdot}10^{-6}$), whereas all other parameters (growth, shrinkage, rescue frequency, pause frequency) are unaffected (Fig. 2*B*).

A close inspection of kymographs suggested that suppression of catastrophes might depend on the number of plus-end–tracking Kif15 motors: in cases where a bright hKif15-eGFP signal (indicating a high local hKif15-eGFP concentration) had accumulated at the tip, catastrophe appeared to be inhibited, leading to extended periods of growth (Fig. 2*A*, kymographs labeled "high"). In case only a dim hKif15-eGFP signal is present at the tip, catastrophe events can occur, which leads to the dissociation of the tracking motor(s) (Fig. 2*A*, kymographs labeled "low"). To further document this effect, we correlated the catastrophe frequency to the intensity of hKif15-eGFP at the plus-end. For this, we subsampled our data by producing intensity line scans along the plus-ends of growth phases (see scheme Fig. 2*C*, *Left*). We then divided all growth phases into coherent phases (>5 seconds) without ("*nil*," orange phases in the schematic kymograph) and with eGFP signal (green phases in the schematic kymograph). The absence of hKif15-eGFP at the growing plus-end was defined by a threshold (orange dotted line in the schematic line scan) derived from line scans along shrinking plus-ends, where hKif15-eGFP is known to be absent (see above). We then calculated the median eGFP intensities over time for each eGFP-positive phase, which gave rise to a split intensity distribution giving a low and high intensity population (Fig. 2*C*, *Middle*). Using this approach, all growth phases were designated as nil, low, or high with respect to the amount of plus-end–tracking eGFP signal. Based on the average intensity of a hKif15-eGFP tetramer (Fig. S2*E*), the low signal population is equivalent to the presence of one or two Kif15 tetramers (median over time) at the plus-end. In the case of the "high" signal population, there would be at least three end-tracking hKif15 tetramers (median over time). Next, we calculated the catastrophe frequency for nil, low, and high plus-end concentrations of hKif15-eGFP. Strikingly, catastrophes are completely absent in phases that maintained high hKif15-eGFP concentrations (over time) at the plus-end (Fig. 2*C*, *Right*). Phases that display a low number of motors (over time) still exhibit catastrophes, but their frequency is already halved compared with the nil population.

In summary, these data demonstrate that collectives of hKif15 motors are able to specifically inhibit catastrophe without affecting any other aspect of microtubule dynamics. Importantly, this anti-catastrophe function requires that a certain threshold of motors (approximately three tetramers) has accumulated at the microtubule tip and tracks the tip during polymerization. Hence we would expect that interfering with hKif15 motor motility would also abolish its anti-catastrophe properties. We therefore determined the global catastrophe rate in the presence of 1.7 mM AMP-PNP, and indeed catastrophe rates were indistinguishable from those of the control (Fig. S3). Finally, the dependency of the anti-catastrophe effect on motor number and motor end tracking predicts that the probability of catastrophe being suppressed will correlate with the length of the microtubule: i.e., the longer the microtubule, the more motors it will collect per time interval [see also the "antenna model" for Kip3 (17, 18)] and the higher the anti-catastrophe effect. Hence we determined the average GFP intensity and the catastrophe rate per growth phase and compared them to the average overall length of the microtubule during that phase (minus to plus end including seed). This analysis shows that short microtubules, on average, display no end-tracking motors and the catastrophe frequency is comparable to that of the control. However, as microtubule length increases, the catastrophe frequency drops significantly with a simultaneous increase in end-tracking eGFP signal (Fig. 2 *D* and *E*). These data show that hKif15 motors can impose length-dependent control on microtubule dynamics.

Microtubule Transport by Kif15 Motors. Previously, we demonstrated that hKif15 can cross-link GMP-CPP–stabilized microtubules (12). We were therefore keen to understand how hKif15 motors operate when dynamic microtubules generate new "intersections." These can be both incomplete (T-shaped; "end-on," Fig. 3*A*; Movies S1.1 and S1.2) or complete (X-shaped, "full intersection," Fig. 3*A*; Movies S1.3 and S1.4). In both situations, we observed that hKif15 motors accumulate at the intersection and eventually drive the transport of one dynamic microtubule along a second microtubule (Fig. 3*A* and Movie S1). We designate the former microtubule as the "cargo" because it is clearly displaced relative to the second microtubule showing no significant displacement (the substrate; see also *Materials and Methods*). During transport the cross-linked substrate and cargo microtubules remain fully dynamic, as exemplified by the cargo microtubule in Fig. 3*A* and Movie S1.1. Because the microtubule seeds are fixed onto the coverslip, transport of the cargo microtubule along the substrate microtubule may result in (extensive) bending of the cargo microtubule (Fig. 3*A* and Movie S1.2). As judged by varying particle intensities, multiple Kif15 motors may contribute to transport (Fig. 3 *A* and *C*; Fig. S4) and accumulate at the intersection once it has been assembled by end-tracking motors (see above) and/or single motors that approach the intersection from the lattice of both substrate and cargo microtubules (see intensity increase of the transport particle in Fig. 3*A* and Movies S1.1 and S2.2; also compare with intensities of single hKif15eGFP tetramers, blue arrows in Fig. 3*A*). We further observed that motors are able to disperse from such a hKif15 collective during or after transport episodes (Fig. S4*B* and Movie S3), arguing that these represent a dynamic assembly. However, such dispersion events are rather infrequent due to the high affinity of hKif15 motors to microtubule overlaps. This is exemplified when observing extensive microtubule overlaps, which recruit multiple motors and do not exhibit any sliding/transport (see *Formation of Parallel Microtubule Arrays by hKif15*). Overall, our data suggest that hKif15 motors might cooperate within a dynamic collective to drive microtubule transport at intersections.

Collective Motility of Kif15 Motors. Our finding that cooperation of hKif15 motors at the microtubule plus-end regulates the frequency of catastrophe raises the possibility that motor numbers may also influence transport behavior. Due to the decline in transport velocity over time (Fig. 3*C*) and the variations in size of motor collectives over time (see above), we focused our analysis on the initial phase of microtubule transport. Kymographs from line scans along the substrate microtubule in the direction of hKif15-eGFP particle movement (Fig. 3 *B* and *C*) show a clear difference in the behavior of low-intensity and high-intensity particles: particles with an intensity of ≤10,000 arbitrary units [corresponding to one or two tetramers (Fig. 3*D* and Fig. S2*E*)] exhibit a behavior similar to the free-running motor characterized by a fast maximal velocity on the substrate microtubule (V_{sub}) during transport, switches between diffusive movement and processive movement, and pauses during a run (Fig. 3*C*, kymographs marked blue; compare with ref. 12 and Fig. S2*A*). In contrast, high-intensity particles [up to ∼11 tetramers (Fig. 3*D* and Fig. S2*E*)] undergo uniform movement, but at a significantly reduced velocity (Fig. 3*C*, kymographs marked green). Overall, the maximal velocities during transport decay exponentially with increasing particle intensity (Fig. 3*D*). However, a recent description of a similar microtubule transport process mediated by artificial adducts of kinesins and plus-end–tracking proteins showed that the maximal transport velocities are affected by the intersection geometry (19, 20). We therefore checked whether the length of the cargo microtubule (the force that is needed to bend a microtubule decreases with its length) or the angle at which cargo and substrate microtubule meet has any influence on the maximal transport velocity in our setup. These analyses show that neither

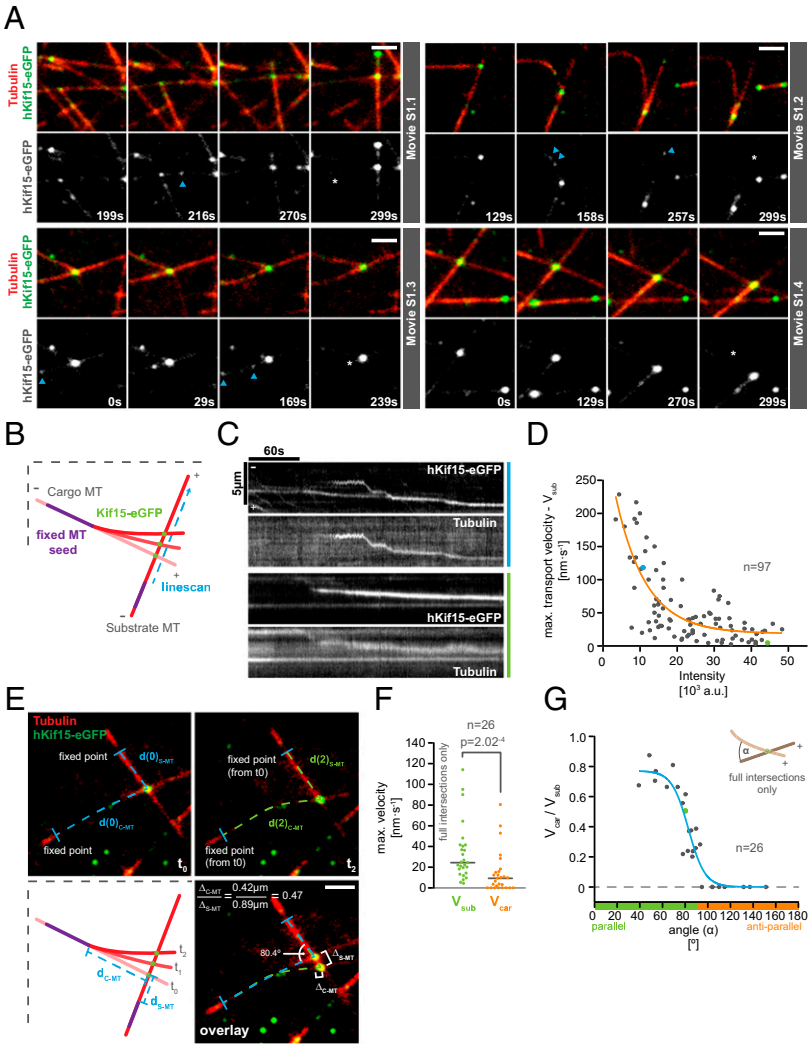

Fig. 3. Characteristics of microtubule transport by hKif15 collectives. (*A*) Selected stills of Movies S1.1–1.4. Transport can occur at "end-on" microtubule intersections (Movie S1.1 and S1.2) or at "full intersections" (Movie S1.3 and S1.4) whereby end-on arrangements may convert into full intersections over time (Movie S1.1). Note the intensity difference between transporting hKif15-eGFP collectives and single tetramers moving on the microtubule lattice (blue arrowheads). Also note that their size can increase over time as further motors approach the intersection (see intensity increase in Movie S1.1). The white asterisk in the last still of the respective movie indicates the start position of the motors as seen in the first frame. (Scale bar, 2 µm.) (*B*) Scheme of a transport event to illustrate how the kymographs for *C* were generated (see also text and *Materials and Methods*). (*C*) Kymographs showing the trajectories of transporting hKif15-eGFP particles (hKif15-eGFP) and the transported cargo microtubule (tubulin) along the substrate microtubule. Background in the tubulin channel is generated by the substrate microtubule. Colors designate motor particles of low (blue) and high (green) intensities. (*D*) Graph showing the negative correlation between the maximal velocity on the substrate microtubule (V_{sub}) during transport and the intensity of the transporting hKif15-eGFP particle. Colored data points indicate the respective transport event shown in *C*. The orange line represents an exponential decay fit: $R^2 = 0.6$. (*E*) Scheme and one example depicting the measurements taken to calculate the simultaneous velocities of a hKif15-eGFP (green) particle on the cargo (V_{car}) and the substrate microtubule (red, V_{sub}) (see also *Materials and Methods*). Blue lines define a fixed point at time point 0; the dashed lines define the respective microtubule contours. (*F*) Graph showing the maximal velocities of hKif15-eGFP motors/motor collectives on the substrate (V_{sub}) and the respective corresponding cargo microtubules (V_{car}). Note that the median velocity on the substrate microtubule is about threefold higher than on the cargo microtubule; i.e., a velocity differential exists across the motor domain pairs of a hKif15 tetramer. The *P* value is derived from a Mann–Whitney *U*-test. Only "full" intersections were analyzed. (*G*) Plot showing the correlation between the velocity differential (i.e., V_{car}/V_{sub} of the same particle) and the angle α between the minus ends of the cross-linked microtubules. A value of 1 means that the motor moves on the cargo microtubule as fast as on the substrate microtubule. A value of 0 infers that the particle does not move at all on the cargo microtubule, although it still shows motility on the substrate microtubule (*F*). The blue line is a sigmodial fit: $R^2 = 0.87$. The green data point identifies the example shown in *E*. Only full intersections were analyzed. Note that this analysis addresses the coordination across the two motor domain pairs of a tetramer in dependency of the intersection geometry. This aspect is different from the previous analysis shown in Fig. S5, which addresses the movement of hKif15-eGFP particles on the substrate microtubule (V_{sub}) only.

parameter significantly affects hKif15 transport behavior (Fig. S5 *A–D*). We thus conclude that single motors interact/interfere with each other during transport, leading to synchronized and uniform but slow collective motility of hKif15 motors.

Kif15 Motors Can Only Translocate on Two Microtubules Simultaneously When They Are in a Parallel Orientation. Movie S1 suggests a simple transport mechanism, i.e., a stable association of hKif15 with the cargo microtubule and motility on the substrate microtubule. In our previous work transport occurred when hKif15 had dwelled at the plus-end of the cargo microtubule, while it walked toward the plus-end of the substrate microtubule (12). However, in our dynamic microtubule setup, hKif15 motors can be also associated with the microtubule lattice of the cargo microtubule during

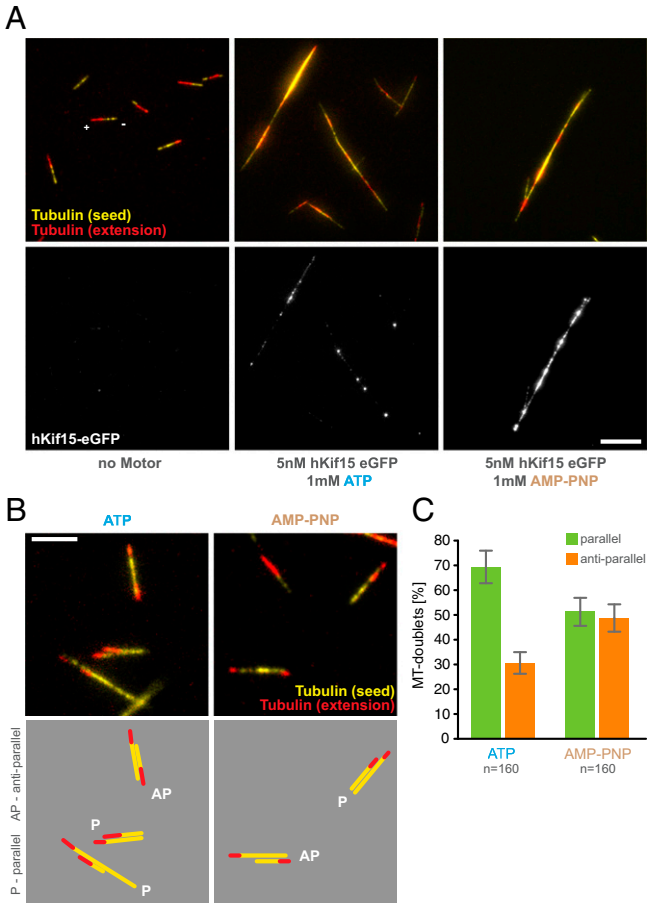

Fig. 4. hKif15 motors assemble microtubules into parallel bundles. (*A*, *Upper*) The formation of complex microtubule bundles from polarity-marked GMP-CPP–stabilized microtubules in the presence of 5 nM hKif15-eGFP and 1.7 mM ATP or AMP-PNP (*Center* and *Right*). Bundling is absent in the no-motor MOCK control (*Left*). Tubulin is shown in false colors for better visibility: HiLyte 647 seeds (corresponding to the minus end) are depicted in yellow, X-rhodamine–labeled extensions (corresponding to the plus end) are in red. (*Lower*) hKif15-eGFP in the corresponding green channel. (Scale bar, 10 μm.) (*B*) Microtubule doublets formed in the presence of 5 nM hKif15-eGFP and 1.7 mM ATP or AMP-PNP. Color coding of the microtubules as in *A*. (Scale bar, 5 μm.) (*Lower*) Graphical depiction of the microtubule orientation within the doublets; P, parallel; AP, antiparallel. (*C*) Quantification of the orientation within microtubule doublets formed in the presence of 5 nM hKif15-eGFP and 1.7 mM ATP or AMP-PNP. Error bars indicate the counting error (square root of *n*).

transport (i.e., at full intersections). This raises a key question: How can a hKif15 tetramer drive transport of cross-linked microtubules, given that it is free to step along both microtubules at the same time? To address this question, we compared movement of hKif15-eGFP (single or multiple motors) on both the cargo and the substrate microtubule over time. We manually measured the distances from a fixed point (the proximal seed end) of each microtubule to the center of the hKif15eGFP signal at several time points during the transport event (Fig. 3*E*) and determined the maximal motor velocity on each microtubule by linear fits (V_{sub} and V_{car}). It became apparent that Kif15 motors indeed move simultaneously on both microtubules that they cross-link. However, movement on one microtubule (the substrate) was significantly faster than movement on the other (the cargo) microtubule ($V_{sub} > V_{car}$, Fig. 3 *E* and *F*). This velocity differential allows relative microtubule transport, even though the motors are translocating on both microtubules at the same time.

However, in one-third of the observed cases, the motor(s) were not moving on the cargo microtubule at all. One could argue that Kif15 tetramers do not cross-link microtubules by their two motor domain pairs but by one motor domain pair and the recently reported putative second microtubule-binding site within the Kif15 stalk (13). In that case, motor-driven movement along the substrate microtubule would passively drag the diffusive second microtubule-binding domain along the substrate microtubule. This would explain why velocities on the cargo microtubule are smaller than on the substrate microtubule or even zero. Alternatively, one could imagine that there are unfavorable microtubule geometries that prevent coordinated stepping on both microtubules.

Thus, a careful analysis of how microtubule geometry influences transport could discriminate between these options: if a freely diffusible secondary microtubule-binding domain is passively dragged along the cargo microtubule, we would predict that the velocity on the cargo microtubule will be high at acute and obtuse angles and minimal around 90° (Fig. S6*A*, I). However, if the motor uses both motor domain pairs to move on the cross-linked microtubules and is adapted to a parallel microtubule geometry, coordinated movement would be possible at angles <90°, but would likely be impaired for angles >90° (Fig. S6*A*, II). As the velocity of hKif15 motor collectives depends on their size, we calculated the relative motor velocity (i.e., V_{car} divided by V_{sub}) to allow a comparison of single motors and collectives different in size. This analysis shows that the velocity (of motor domains) on the cargo microtubule is comparable to that on the substrate microtubule when intersecting microtubules are at an acute angle. As the angle exceeds 60° the velocity on the cargo microtubule rapidly drops, and no motility is observed for angles above 90° (i.e., antiparallel microtubule orientation) (Fig. 3*G*). This velocity ratio does not depend on the intensity of the particle, the velocity on the substrate microtubule, or the microtubule length between seed end and intersection (Fig. S6 *B–E*). These data suggest that hKif15 motors actively walk on both microtubules that they cross-link and drive relative microtubule transport via a velocity differential across both motor domain pairs. This behavior is influenced by the geometry of intersecting microtubules with an antiparallel microtubule arrangement preventing coordinated stepping of the domain pairs, but still allows canonical microtubule transport along the substrate microtubule (i.e., the motor is firmly attached to one microtubule while it is stepping on the other). When intersecting microtubules are parallel, however, hKif15 motors can drive (biased) parallel sliding (i.e., the motor simultaneously steps on both microtubules that it cross-links).

Formation of Parallel Microtubule Arrays by hKif15. In human cells, hKif15 is largely localized to parallel microtubule bundles (11, 21). Thus, it might be possible that hKif15 uses geometry-dependent transport and (biased) parallel sliding to autonomously drive formation of parallel bundles. To test this, we perfused blocked microscopy chambers with a mix of free polarity-marked, GMP-CPP–stabilized microtubules and 5 mM hKif15-eGFP in the presence of 1.7 mM ATP. After preincubation for 5 min at 25 °C, a series of single TIRF images were taken. Fig. 4*A* shows that hKif15 motors indeed can drive the formation of large microtubule bundles over time. Bundling per se does not depend on motor activity as hKif15-eGFP motors still bundle microtubules in the presence of 1.7 mM AMP-PNP, which locks the motor immotile on the microtubule lattice (Fig. 4*A*; see also Fig. 1*A* and Fig. S3 for motor behavior in the presence of AMP-PNP). Next we analyzed the geometry of hKif15-eGFP–derived microtubule bundles. For this we determined the relative orientation of microtubules within microtubule doublets based on the polarity marks and the relative intensity increase in microtubule overlaps (Fig. 4*B*). hKif15-eGFP motors mainly formed parallel microtubule doublets with a bias of 70% (Fig. 4 *B* and

C). This orientation bias is lost completely in doublets formed in the presence of AMP-PNP (Fig. 4 *B* and *C*), suggesting that the motor activity (and therefore microtubule transport/focusing) is essential to establish parallel bundles, which is consistent with the in vivo localization of the motor. We note that once the bundle has formed and hKif15 motors have accumulated strongly within, no lateral sliding/relative microtubule movement can be observed (Fig. S7*B*). Thus, in line with our previous experiments, hKif15 motors act as a static cross-linker once they have accumulated in sufficient numbers on extensive overlaps. hKif15 thereby prevents the disintegration of established bundles by continuous parallel sliding.

Discussion

Based on the in vitro data in this study we propose that Kif15 will be able to drive the self-organization of parallel microtubule bundles with synchronized dynamics (see a summarizing animation in Movie S4). This progresses our understanding of how hKif15 motors may operate during mitosis to promote the assembly and maintenance of a bipolar spindle (see below).

We show that single hKif15 motors or small collectives of up to ~11 motors (based on the average intensity of a hKif15-eGFP tetramer; Fig. S2*E*) can drive relative microtubule–microtubule transport at (incomplete) microtubule intersections that occasionally form among dynamic microtubules. After an intersection has been established, processive hKif15 motors accumulate at these intersections either as a result of motors walking up to an intersection or by plus-end–tracking motors that already had been deposited there during formation of the intersection. In case of an incomplete "end-on" intersection, hKif15-driven transport is reminiscent of microtubule steering/guidance described for artificial adducts of plus-end–binding proteins and kinesins (19, 20). However, hKif15 integrates all essential activities—plus-end tracking, cross-linking, and processive motility—into a single bivalent motor that can operate as an autarkic functional unit. Furthermore, hKif15 motors are able to walk on both microtubules that they cross-link and drive microtubule transport also at full intersections by a velocity differential between both motor domain pairs (i.e., the pair bound to the cargo microtubule moves slower than that on the substrate microtubule). This differential is independent from motor number, but depends on the geometry of the cross-linked microtubules: it is maximal for obtuse angles >90° (i.e., an antiparallel microtubule arrangement) and minimal for acute angles (i.e., a parallel microtubule orientation). We note that in our experimental setup (like in the living cell) microtubule freedom is restricted by fixed points (fixed seeds or microtubule–microtubule intersections other than the transport intersection).

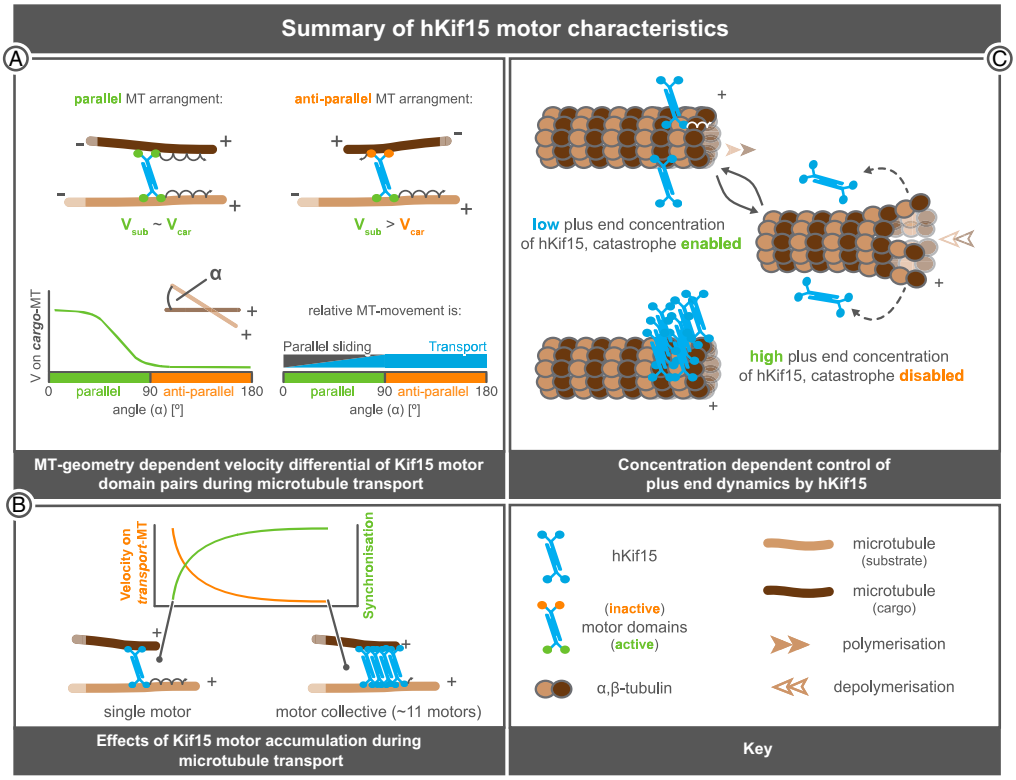

Fig. 5. Functional properties of hKif15 motors. (*A*) The relative velocity of hKif15 motor domain pairs on the microtubules that hKif15 cross-links depends on the underlying microtubule geometry. In parallel arrangements (*Top* and *Bottom Left* with the angle in between the minus ends: α→0°) velocities on the substrate (V_{sub}) and on the cargo microtubule (V_{car}) are approximately equal (V_{sub}~V_{car}); motors will then move to the plus-end of both microtubules. With increasing angles (α→90°; *Bottom Left*) the relative velocity on one of the cross-linked microtubules (the cargo microtubule) drops (V_{car}→0). Thus, the relative microtubule movement in parallel arrangements can be described as biased parallel sliding (*Bottom Right*). In antiparallel microtubule arrangements (α>90°, *Top Right* and *Bottom Left*) motors completely stall on the cargo microtubule. The result is canonical transport of the cargo microtubule along the substrate microtubule (*Top Right*). This behavior means that there is a continuum between parallel sliding and transport as the orientation of the microtubules changes (*Bottom Right*). (*B*) hKif15 motors within collectives interfere with each other during microtubule transport. With increasing numbers of motors, the movement is synchronized (steady processive movement at the same velocity without pauses) at the cost of overall velocity of the collective. (*C*) hKif15 motors cooperate to suppress catastrophes at the microtubule plus-ends. At low hKif15 plus-end concentrations catastrophes are enabled (*Top*), but might occur at reduced frequency. Once a catastrophe occurs, hKif15 motors are stripped from the microtubule lattice as they fail to bind to curved protofilaments (*Middle*). However, as a certain threshold of motors has accumulated at the plus tip (more than three motors in time average) catastrophes are fully suppressed (*Bottom*). Continuous suppression of catastrophes on polymerizing microtubules needs the active (ATP-dependent) plus-end tracking of motors. We note that the illustration of the motor geometry/polarity of hKif15 tetramers is speculative as no structural information is available yet.

These restrictions might differentially influence the translocation of motor domains along the cross-linked microtubules, although we did not find any evidence for this in our data. In summary, hKif15-driven microtubule motility at intersections can be described as canonical transport for obtuse angles (180°–90°) and biased parallel sliding for acute angles (90°–0°) that gradually loses its bias with decreasing angles. This way, hKif15 motors will drive extensive rearrangements/transport of antiparallel microtubules, whereas it would just walk to the tips of perfectly aligned parallel microtubules without driving any relative microtubule transport (Fig. 5*A*). As a consequence, antiparallel microtubule arrangements will be resolved and cross-linked microtubules will be arranged into a (more or less parallel) configuration with hKif15 at their tips. We note that, due to this mechanism, the motor activity of hKif15 is crucial to the directional bias within the formed microtubule bundle, in contrast to antiparallel microtubule bundling by the *Drosophila* Eg5 homolog KLP61F, which depends on structural determinants within the motor itself (22).

Although structural determinants within the hKif15 tetramer are likely to be the cause for the observed velocity differential at full intersections, we can only speculate whether hKif15 tetramers are parallel monopolar, antiparallel bipolar, or parallel bipolar without any structural information (Fig. S8*A*). Parallel monopolar tetramers could cross-link microtubules by a second ATP-independent microtubule-binding site, which has been proposed recently (13). In this case, the velocity differential would be generated by unequal distribution of motor domains between the cross-linked microtubules (Fig. S8*B*). However, such a model predicts that the velocity differential would be insensitive to the microtubule geometry. This is not supported by our data. In case of a bipolar tetramer topology (with a low torsional compliance), a change in the microtubule angle would twist the tetramer, which might impair the stepping of one motor domain pair sterically. We currently favor this idea because it has recently been shown that the dimeric rice Kinesin-14 OsKHC1, which cross-links actin filaments and microtubules, is subject to such an effect. OsKHC1 moves at different velocities on the microtubule depending on the relative orientation of the polar actin filaments to which it is attached (23). It remains unclear why such torsion would affect one pair of motor domains in a Kif15 tetramer over the others. However, this could be explained if the topology of the cross-linking tetramer was parallel bipolar: in such an arrangement, the stalk might act as a symmetry breaker (Fig. S8*C*). Consistent with this idea, the symmetric antiparallel bipolar Eg5 motor does not show any (angle-dependent) velocity differential on the microtubules that it cross-links (5, 6).

During transport, the collective behavior of Kif15 results in the synchronization of motor movements at the cost of overall motor velocity (Fig. 5*B*, in contrast to the movement of single "free" motors, which alternate between processive runs, pauses, and diffusive motion) (12). Such negative correlation between motor numbers and overall collective velocity has also been described for mechanically coupled conventional kinesins (24). In the case of hKif15 collectives, mechanical coupling might be achieved by the physical linkage to the same cargo microtubule or to other motors within the collective. However, we observed (rare) situations where the cargo microtubule detached after transport had been initiated and hKif15 collectives often continued synchronous movement, without changing their velocity or size dramatically (Fig. S4*A* and Movie S2). This might suggest a physical coupling of motors within the collective.

These biophysical properties reveal that hKif15 motors—although functionally redundant with Eg5 in terms of spindle assembly/maintenance—are mechanistically distinct: hKif15 motors are biophysically adapted to bind to parallel overlaps and actively drive the formation of parallel bundles irrespective of the initial microtubule orientation by a transport/parallel sliding mechanism. However, hKif15 cannot drive the coordinated relative extensile sliding of antiparallel overlaps (see also below). Eg5 in stark contrast is adapted to drive the extensile microtubule sliding of antiparallel overlaps and stabilizes parallel overlaps. As a result, Eg5 will catalyze the formation of parallel microtubule bundles through the selective destabilization of antiparallel overlaps. This mechanism, however, requires the random occurrence of parallel microtubule overlaps. We therefore propose that the main task of hKif15 motors in vivo is to actively reorganize microtubules into parallel bundles. This would be consistent with the reported enrichment of hKif15 motors to kinetochore fibers (9–11). Furthermore, depletion of hKif15 reduces k-fiber length in vivo (11). Thus, we speculate that hKif15 shapes and stabilizes the kinetochore fiber to maintain overall spindle integrity.

Although adapted to parallel microtubule geometry, hKif15 motors efficiently accumulate in large numbers at microtubule overlaps of any geometry. Due to the inverse correlation between motor numbers and velocity of a mechanically coupled collective, large hKif15 collectives appear to be immobilized within extensive overlaps, unable to support any form of lateral microtubule sliding. Therefore, hKif15 cannot drive centrosome separation during prophase like Eg5 (9, 10), which would require extensile sliding of antiparallel microtubule overlaps. In contrast, accumulation of (slow moving or even stalling) hKif15 motor collectives in antiparallel overlaps of interpolar microtubules would rather create drag in the extensile system. This property could, however, explain how hKif15 motors counteract Eg5-dependent forces in vivo (11). This drag effect is likely to be intensified in vivo as hKif15 can physically interact with the microtubule-associated protein hTpx2, which switches the motor into a state that can withstand even higher loads (12).

Our data further show that cooperative behavior of hKif15 motors is not restricted to microtubule transport, as it is also essential to bring about the suppression of catastrophe. Dynamic end-tracking and catastrophe suppression by hKif15 might be of particular importance to its transport and focusing [and thus also indirectly for the bundling (Movie S4)] capacities, as both properties positively influence the end residency time of the motor on dynamic microtubules (see also below), a parameter shown to be crucial for microtubule focusing by multipolar/bipolar motors (25). One possible mechanism for catastrophe suppression by hKif15 would be that the collective of hKif15 tetramers could dynamically cross-link neighboring protofilaments during outgrowth of the microtubule (Fig. 5*C*), acting like a processive clamp that follows the growing tip. In this way, hKif15 collectives would stabilize lateral protofilament interactions and prevent the unpeeling of single protofilaments (15), which might explain the observed threshold. According to the "antenna model," the accumulation of motors at the tip is proportional to the length of the microtubule. As a result, the longer a microtubule becomes, the more likely it is that its tip accumulates sufficient hKif15 motor to inhibit catastrophe. Interestingly, the length-dependent plus-end accumulation of hKif15 motors is additionally modified by the underlying microtubule dynamics, as all end-tracking hKif15 motors are stripped off the tip in case catastrophes are still allowed to occur. Thus, the length-dependent catastrophe suppression by hKif15 motors is partly reminiscent of the length-dependent increase in depolymerization activity of Kinesin-8 motors caused by plus-end accumulation of motors (17, 18). Hence, Kinesin-12 motors might be functional antagonists of Kinesin-8 motors, and both motors could be important for regulating the distribution of microtubule lengths within the mitotic spindle. It will be interesting to test whether these two motor types indeed operate together to control the length distribution of a microtubule population.

In principle, hKif15 collectives might be able to synchronize the dynamics of all microtubules within a parallel bundle. Like that, it is possible that hKif15 would contribute to the control of microtubule plus-end dynamics at the kinetochore; in this regard

hKif15 has also been reported to localize to kinetochores (11) and influence chromosome movement (21). Promoting microtubule growth in the kinetochore fiber can indirectly create outward-pushing forces on the centrosome to assist spindle elongation. In fact, overexpression of hKif15 (in the absence of Eg5) can promote bipolar spindle assembly via the so-called "prometaphase pathway" (11), which is known to require kinetochore-generated pushing forces (26).

Outside of mammals, these hKif15-dependent mechanisms are also consistent with the idea that Xklp2 (*Xenopus* Kinesin-12) is required for maintaining spindle bipolarity by holding centrosomes apart (27, 28). Moreover, the capacity of hKif15 to drive formation of parallel bundles could explain the reported role for *Caenorhabditis elegans* Kinesin-12 (KLP-18) in converting disordered microtubules that are present around meiotic chromosomes into an ordered parallel array (29, 30). Intriguingly, Kinesin-12s may have more diverse roles with emerging evidence suggesting that these motors are important for shaping parallel microtubule arrays within developing neuronal axons (31) and execution of cytokinesis in angiosperms (32–34). Thus, the capacity for Kinesin-12 family members to remodel dynamic microtubule networks is likely to be crucial in multiple biological systems, and it will be interesting to investigate whether they use the same mechanism.

Materials and Methods

Protein Purification. His_6-hKif15 and His_6-hKif15-eGFP were expressed and purified from SF9-insect cells as described previously (12). His_6-Eg5 was expressed from a FastBac-M13 plasmid, in which the Eg5 ORF was inserted via the SalI and SpeI sites of the multiple cloning site. Purification was performed as for hKif15 constructs. Protein preparations were analyzed on SDS/PAGE to assess their purity (Fig. S1*A*). Concentrations were determined against a BSA standard run on the same SDS PAGE gel using ImageJ.

Microtubule Sedimentation Assays. Taxol-stabilized microtubules were grown from purified pig brain tubulin in BRB80 (80 mM Pipes pH 6.8, 1 mM $MgCl_2$, 1 mM EGTA) and 1 mM GTP by incremental addition of taxol to 10 μM for 1 h at 37 °C. Polymerized microtubules were washed once with BRB80 containing 10 μM taxol using a Beckman Airfuge and resuspended in sedimentation buffer (35 mM sodium phosphate buffer, pH 7.0, 1 mM $MgCl_2$, 1 mM EGTA, 1 mM DTT, 10 mM Taxol). Vinblastine-induced tubulin curls were grown from 10 mM purified tubulin in 1 mM MES buffer, pH 6.4, 1 mM $MgCl_2$, 1 mM EGTA, 1 mM DTT using 10 μM vinblastine (Sigma-Aldrich), and 1 mM GTP for 1 h at 37 °C. Curls were washed once with polymerization buffer and resuspended in sedimentation buffer plus 10 μM vinblastine. Motors were precleared in sedimentation buffer for 10 min at 45,000 × *g* in a TLA100 rotor (Beckman) using thick-wall poly-allomer tubes. hKif15 and Eg5 motors (16.5 nM each, calculated for the respective tetramer) then were mixed with the indicated amount of tubulin and incubated for 20 min at room temperature in the presence of 2 mM AMP-PNP. Samples were spun for 20 min at 45,000 × *g* and 25 °C (as above). The supernatants were TCA-precipitated and analyzed with their respective resuspended pellets by SDS/PAGE. Microtubules and vinblastine-induced tubulin curls exhibit reduced stability in 35 mM sodium phosphate buffer so that partial depolymerization occurred, which gave rise to the horizontal error bars in Fig. S1*E*. The percentage of sedimented tubulin and cosedimented hKif15 was quantified using ImageJ. hKif15 values were corrected for background sedimentation in the "no tubulin" control. To check polymer morphology, samples were transferred to glow-discharged carbon-coated grids and stained with 2% uranium acetate. Images were acquired on a JEOL 2010F 200 kV electron microscope (JEOL U.K.) equipped with a Gatan Ultrascan 4000 CCD camera (Gatan U.K.).

TIRF Microscopy. Flow chamber setup and coverslip preparation were essentially performed as in ref. 12. For our dynamic microtubule assay the glass surface was coated with poly-L-lysine-poly-ethylene-glycol-biotin (Surface-Solutions), activated with 1 mg/mL streptavidin, and blocked with 1 mg/mL κ-casein. Short GMP-CPP (Jena BioSciences)–stabilized microtubules labeled 1:30 with biotin and HiLyte647 (Cytoskeleton) were allowed to bind to the activated surface. The chamber was perfused with the assay mix (with or without 5 nM hKif15-eGFP tetramers), which had been precleared for 5 min in an Airfuge at 4 °C and then sealed with VALAP. The assay contained 60 mM Pipes, pH 6.8, 4 mM $MgCl_2$, 1 mM EGTA, 1.3 mM GTP, 1.7 mM ATP/ADP/AMP-PNP, 5.3 mM DTT, 67 mM glucose, 0.27 mg/mL catalase, 0.54 mg/mL glucose oxidase, 0.8 mg/mL κ-casein, 0.25% methyl cellulose, and X-rhodamine (Cytoskeleton) and nonlabeled pig brain tubulin in the ratio 1:10. Chambers were imaged at 35 °C on an Olympus CELLR/TIRF microscope (Olympus) equipped with an ImagEM emCCD camera (Hamamatsu Photonics), an environmental chamber, and a stage-top incubator (Okolab) using a 100× N.A. 1.49 objective with 1.6× auxiliary magnification.

Five-minute dual-color time-lapse movies were recorded at 1 frame per second using a 488-nm (150-ms exposure) and a 561-nm (80- to 100-ms exposure) laser line to visualize the eGFP-tagged motors and the X-rhodamine–labeled dynamic microtubules. The position of HiLyte647-labeled seeds was captured before and after each time-lapse movie using the 640-nm laser lines at an 80-ms exposure. Movies were analyzed and processed with ImageJ. Kymographs were produced by the MultipleKymograph plugin (www.embl.de/eamnet/html/body_kymograph.html). Motor speeds and microtubule dynamics were manually determined with imageJ from these kymographs. To observe and reliably quantify the bundling of free GMP-CPP–stabilized polarity-labeled microtubules, a flow cell blocked with Pluronic F127 (Sigma-Aldrich) and κ-Casein was perfused with polarity-labeled microtubules (i.e., X-rhodamine–labeled extensions grown from HiLyte 674-labeled seeds) mixed with 5 nM tetrameric hKif15 in the presence of 1.7 mM ATP or AMP-PNP. After a 5-min preincubation time at 25 °C, single-frame pictures were taken at the same temperature, using the 488-nm (150-ms exposure), the 561-nm (80-ms exposure), and the 640-nm laser line (80-ms exposure). TIRF setup and buffer conditions were as for the experiments with dynamic microtubules. For quantification, only microtubule doublets were analyzed using location of the polarity marks and the relative increase of fluorescence intensity in microtubule overlaps.

The behavior and bleaching of single hKif15 motors were essentially monitored as outlined (12), but with four frames per second and an exposure of 150 ms by the 488-nm laser line in BRB60 at 35 °C.

Analysis of Microtubule Dynamicity. Parameters of microtubule dynamicity were extracted manually from kymographs using ImageJ. The following definitions were used: catastrophe frequency—number of catastrophe events divided by the total time of growth; rescue frequency—number of rescue events divided by the total time of shrinkage; pause frequency—number of pauses divided by the total shrinkage and growth time; and pause—phases with changes in microtubule length <0.05 μm·min^{-1}. The probability values given in Fig. 2*B* were derived from a Mann–Whitney *U* test. The SE of mean was calculated from the mean of the respective values per microtubule.

Measurement of Transport Velocities. In general, transport velocities were extracted from kymographs derived from line-scans along the substrate microtubule using ImageJ (see also above). Important criteria for analysis were: first, to accurately measure the velocity from kymographs, the substrate microtubule must not move or bend significantly during the transport event. In our setup, the "substrate microtubules" were fixed because the transport event took place on (*i*) a seed that was coupled to the surface through streptavidin–biotin linkages (rare), (*ii*) a segment between a fixed seed and a stable microtubule–microtubule intersection further "upstream" of the event being followed (frequent), or (*iii*) a rigid microtubule–microtubule doublet (rare). Second, to avoid measuring false transport events (i.e., coincidental, not motor-driven movement of the microtubule in the same direction as motor movement), the trajectories of the cargo microtubule and the driving motor must match exactly.

To measure the differential velocities on cargo and substrate microtubules (V_{car} and V_{sub}), splines were fitted to the distance from a fixed point between the distal end of the microtubule seed and the transporting hKif15 particle using ImageJ. The fixed point can be (ordered by preference): the proximal seed end, the distal seed end, an arbitrary point on the seed, or a position-stable intersection in between the proximal seed end and the transporting particle. The changes in distance over time were plotted and the maximal velocity derived from (local) linear fits. Subsequently, the velocity of the cargo microtubule was divided by the velocity of the substrate microtubule to allow comparison of transport events independent of the size of the motor collective. Criteria for analysis were the following: to allow accurate spline fitting, both cargo microtubule and substrate microtubule must be visible from their seeds to the intersection throughout the entire transport event. Due to those criteria and traces that could not be fitted, the number of analyzable events at full intersections for Fig. 3 *F* and *G* and Fig. S6 decreased from 51 (Fig. S5*C*) to 25.

ACKNOWLEDGMENTS. We thank Elina Vladimirou for providing HeLa whole-cell extracts, Ian Hands Portman (University of Warwick, Imaging Suite) for help with electron microscopy, and Richard McIntosh for thoughts on hKif15 binding to curved tubulin filaments. A.D.M. is funded by a Biotechnology and Biological Sciences Research Council (BBSRC) Grant BB/I021353/1 and a Wellcome Trust Senior Investigator Award 106151/Z/14/Z.

1. Cross RA, McAinsh A (2014) Prime movers: The mechanochemistry of mitotic kinesins. *Nat Rev Mol Cell Biol* 15(4):257–271.
2. Tanenbaum ME, Medema RH (2010) Mechanisms of centrosome separation and bipolar spindle assembly. *Dev Cell* 19(6):797–806.
3. Blangy A, et al. (1995) Phosphorylation by p34cdc2 regulates spindle association of human Eg5, a kinesin-related motor essential for bipolar spindle formation in vivo. *Cell* 83(7):1159–1169.
4. Kapoor TM, Mayer TU, Coughlin ML, Mitchison TJ (2000) Probing spindle assembly mechanisms with monastrol, a small molecule inhibitor of the mitotic kinesin, Eg5. *J Cell Biol* 150(5):975–988.
5. Kashina AS, et al. (1996) A bipolar kinesin. *Nature* 379(6562):270–272.
6. Kapitein LC, et al. (2005) The bipolar mitotic kinesin Eg5 moves on both microtubules that it crosslinks. *Nature* 435(7038):114–118.
7. Kapitein LC, et al. (2008) Microtubule cross-linking triggers the directional motility of kinesin-5. *J Cell Biol* 182(3):421–428.
8. van Heesbeen RGHP, Tanenbaum ME, Medema RH (2014) Balanced activity of three mitotic motors is required for bipolar spindle assembly and chromosome segregation. *Cell Rep* 8(4):948–956.
9. Tanenbaum ME, et al. (2009) Kif15 cooperates with eg5 to promote bipolar spindle assembly. *Curr Biol* 19(20):1703–1711.
10. Vanneste D, Takagi M, Imamoto N, Vernos I (2009) The role of Hklp2 in the stabilization and maintenance of spindle bipolarity. *Curr Biol* 19(20):1712–1717.
11. Sturgill EG, Ohi R (2013) Kinesin-12 differentially affects spindle assembly depending on its microtubule substrate. *Curr Biol* 23(14):1280–1290.
12. Drechsler H, McHugh T, Singleton MR, Carter NJ, McAinsh AD (2014) The Kinesin-12 Kif15 is a processive track-switching tetramer. *eLife* 3:e01724.
13. Sturgill EG, et al. (2014) Kinesin-12 Kif15 targets kinetochore fibers through an intrinsic two-step mechanism. *Curr Biol* 24(19):2307–2313.
14. Hancock WO (2014) Mitotic kinesins: A reason to delve into kinesin-12. *Curr Biol* 24(19):R968–R970.
15. Simon JR, Salmon ED (1990) The structure of microtubule ends during the elongation and shortening phases of dynamic instability examined by negative-stain electron microscopy. *J Cell Sci* 96(Pt 4):571–582.
16. Gigant B, et al. (2005) Structural basis for the regulation of tubulin by vinblastine. *Nature* 435(7041):519–522.
17. Varga V, et al. (2006) Yeast kinesin-8 depolymerizes microtubules in a length-dependent manner. *Nat Cell Biol* 8(9):957–962.
18. Varga V, Leduc C, Bormuth V, Diez S, Howard J (2009) Kinesin-8 motors act cooperatively to mediate length-dependent microtubule depolymerization. *Cell* 138(6):1174–1183.
19. Chen Y, Rolls MM, Hancock WO (2014) An EB1-kinesin complex is sufficient to steer microtubule growth in vitro. *Curr Biol* 24(3):316–321.
20. Doodhi H, Katrukha EA, Kapitein LC, Akhmanova A (2014) Mechanical and geometrical constraints control kinesin-based microtubule guidance. *Curr Biol* 24(3):322–328.
21. Vladimirou E, et al. (2013) Nonautonomous movement of chromosomes in mitosis. *Dev Cell* 27(1):60–71.
22. van den Wildenberg SMJL, et al. (2008) The homotetrameric kinesin-5 KLP61F preferentially crosslinks microtubules into antiparallel orientations. *Curr Biol* 18(23):1860–1864.
23. Walter WJ, Machens I, Rafieian F, Diez S (2015) The non-processive rice kinesin-14 OsKCH1 transports actin filaments along microtubules with two distinct velocities. *Nat Plants* 1:15111.
24. Bieling P, Telley IA, Piehler J, Surrey T (2008) Processive kinesins require loose mechanical coupling for efficient collective motility. *EMBO Rep* 9(11):1121–1127.
25. Surrey T, Nedelec F, Leibler S, Karsenti E (2001) Physical properties determining self-organization of motors and microtubules. *Science* 292(5519):1167–1171.
26. Toso A, et al. (2009) Kinetochore-generated pushing forces separate centrosomes during bipolar spindle assembly. *J Cell Biol* 184(3):365–372.
27. Boleti H, Karsenti E, Vernos I (1996) Xklp2, a novel Xenopus centrosomal kinesin-like protein required for centrosome separation during mitosis. *Cell* 84(1):49–59.
28. Walczak CE, Vernos I, Mitchison TJ, Karsenti E, Heald R (1998) A model for the proposed roles of different microtubule-based motor proteins in establishing spindle bipolarity. *Curr Biol* 8(16):903–913.
29. Segbert C, et al. (2003) KLP-18, a Klp2 kinesin, is required for assembly of acentrosomal meiotic spindles in Caenorhabditis elegans. *Mol Biol Cell* 14(11):4458–4469.
30. Connolly AA, et al. (2014) Caenorhabditis elegans oocyte meiotic spindle pole assembly requires microtubule severing and the calponin homology domain protein ASPM-1. *Mol Biol Cell* 25(8):1298–1311.
31. Liu M, et al. (2010) Kinesin-12, a mitotic microtubule-associated motor protein, impacts axonal growth, navigation, and branching. *J Neurosci* 30(44):14896–14906.
32. Lipka E, et al. (2014) The phragmoplast-orienting kinesin-12 class proteins translate the positional information of the preprophase band to establish the cortical division zone in Arabidopsis thaliana. *Plant Cell* 26(6):2617–2632.
33. Müller S, Han S, Smith LG (2006) Two kinesins are involved in the spatial control of cytokinesis in Arabidopsis thaliana. *Curr Biol* 16(9):888–894.
34. Lee Y-RJ, Li Y, Liu B (2007) Two Arabidopsis phragmoplast-associated kinesins play a critical role in cytokinesis during male gametogenesis. *Plant Cell* 19(8):2595–2605.
35. McClelland SE, McAinsh AD (2009) Hydrodynamic analysis of human kinetochore complexes during mitosis. *Methods Mol Biol* 545:81–98.
36. Acar S, et al. (2013) The bipolar assembly domain of the mitotic motor kinesin-5. *Nat Commun* 4:1343.
37. Nédélec FJ, Surrey T, Maggs AC, Leibler S (1997) Self-organization of microtubules and motors. *Nature* 389(6648):305–308.
38. Hentrich C, Surrey T (2010) Microtubule organization by the antagonistic mitotic motors kinesin-5 and kinesin-14. *J Cell Biol* 189(3):465–480.